

Article

GIS-Analysis for Active Tectonics Assessment of Wadi Al-Arish, Egypt

Bashar Bashir ¹, Abdullah Als Salman ¹, Hussein Bachir ² and Mahmoud Elnobi ^{3,*}

¹ Department of Civil Engineering, College of Engineering, King Saud University, P.O. Box 800, Riyadh 11421, Saudi Arabia

² Department of Civil, Geo, and Environmental Engineering, Technical University of Munich, Arcisstrasse 21, 80333 Munich, Germany

³ Department of Geology, Faculty of Science, Al-Azhar University, Cairo 11651, Egypt

* Correspondence: mahmoudalnubi.sci.stu.1@azhar.edu.eg

Abstract: In this paper, we apply an effective method to evaluate relative tectonic activity by applying several morpho-tectonic indices that are useful in evaluating topography and tectonics. These indices include stream length-gradient, asymmetric factor, hypsometric index, hypsometric curves, valley floor width to valley height ratio, drainage basin shape, and mountain front sinuosity. The study region of Wadi Al-Arish in northern Sinai Peninsula in northern Egypt is a natural laboratory to examine relative tectonic activity levels for calculating morpho-tectonic indices of several catchments and sub-catchments rather than an individual catchment. Northern Sinai, comprising the Wadi Al-Arish area, is characterized by several large inversion anticline folds. The cumulative results extracted from morpho-tectonic indices are presented as a new index, namely relative tectonic activity level (RTAL), which we classified into four levels: low, moderate, high, and very high relative tectonic activity. Therefore, the study region provides different levels of relative tectonic activity resulting from fault patterns affecting the northern Sinai inversion forms. The paper examines the concept that regions with various levels of tectonic activity are associated with specific values of RTAL.

Keywords: active tectonics; morphometric indices; relative tectonic activity level; northern Sinai; Egypt



Citation: Bashir, B.; Als Salman, A.; Bachir, H.; Elnobi, M. GIS-Analysis for Active Tectonics Assessment of Wadi Al-Arish, Egypt. *Appl. Sci.* **2023**, *13*, 2659. <https://doi.org/10.3390/app13042659>

Academic Editors: Zdena Dobesova and Vilém Pechanec

Received: 1 January 2023

Revised: 10 February 2023

Accepted: 16 February 2023

Published: 18 February 2023



Copyright: © 2023 by the authors. Licensee MDPI, Basel, Switzerland. This article is an open access article distributed under the terms and conditions of the Creative Commons Attribution (CC BY) license (<https://creativecommons.org/licenses/by/4.0/>).

1. Introduction

Natural phenomena initiated inside the earth and/or near the surface can produce various natural hazards. These include earthquakes, volcanoes, floods, and avalanches [1–4]. Advances in using tectonic geomorphology, remote sensing, and geospatial analytical applications allow fundamental knowledge acquisition in our appreciation of the role of tectonic evolution of active landforms in natural hazard assessment. Globally, catastrophes driven by earthquakes provide significant obstacles to development plans and cause numerous deaths and extensive damage. Seismic hazards in active regions have been investigated and evaluated by many researchers [5–9]. The seismicity of the Mediterranean region has resulted in recent seismic activity and earthquakes. Seismic sequence evolution, fault modeling, and stress transfer methods were applied to investigate the 20 July, 17 Kos-Gökova Gulf earthquakes in SE Aegean [10]. The authors of this study examined the effects of the main shocks and the largest aftershock, and evaluated post-sequence effects by determining the region where static stress increased. This was critical for seismic risk assessment. An earthquake focal prediction mechanism model was applied in Italy by the authors in of [11]. They extracted data from the latest stress map of Italy to initiate an effective model for predicting the next large earthquakes. In Greece, Sentinel-1 SAR data were processed using InSAR techniques to study the co-seismic and post-seismic faulting of the 2021 Northern Thessaly earthquakes [12]. In this model, the authors mapped the co-seismic displacement of the Verdikoussa, Ellassona, Tyrnavos events and the post-seismic displacement accompanied by the Tyrnavos event. In

addition, they calculated the effect of co-seismic Coulomb stress changes resulting from the seismic sequence on the neighboring faults, providing an effective model to assess regional seismic risks. The authors of [6] examined relative active seismic development in southern Spain. They characterized the area into different levels of seismic activity. The Hindu Kush in NW Pakistan and NE Afghanistan is a highly deformed region resulting from an integration of vertical and horizontal motion and interaction between deposition and erosion processes. This region was evaluated using GIS techniques and defined into four classes of tectonic activity [7]. The author of [1] analyzed mountain fronts and river morphology of the Tuz Gölü Fault Zone in central Anatolia to assess earthquake potential and regional seismic hazard along the entire fault. A study of the Abu-Dabbab area in the eastern Desert of Egypt was discussed, and at two potential drivers of seismicity were detected [9]. The evaluation of active spots and uplifting signals over active faults, folds, uplifting catchments can be recognized by detailed investigations of tectonic geomorphology applications. Investigating morpho-tectonic indices, including stream length-gradient (SL), asymmetric factor (Af), hypsometric index (Hi), hypsometric curves (Hc), valley floor width to valley height ratio (Vf), drainage basin shape (Bs), and mountain front sinuosity (Smf), are very powerful tools to assess and partly mitigate most modern natural seismic-hazards.

The Sinai Sub-plate has a complicated deformation at its boundaries with the African, Eurasian, and Arabian plates. Many processes, such as inter-plate vertical and horizontal motion, and intra-plate adjustments between crust and mantle, played a key role in the Sinai sub-plate's geodynamic evolution [13]. These processes accelerated the uplifting and rifting that determined sub-plate active tectonic structures and shaped its morphology in the form of topographic fractures [14]. The Sinai sub-plate is located between latitudes $27^{\circ}45' - 29^{\circ}55'$ and longitudes $32^{\circ}40' - 34^{\circ}50'$ and bounded by the Aqaba and Suez Gulfs from the east and west, respectively. It terminates at the Mediterranean Sea in the north and the Red Sea in the south (Figure 1). The Wadi Al-Arish catchment is the scope of this study which is considered the largest drainage catchment in the Sinai Peninsula, covering parts of Egypt and Palestine.



Figure 1. Google earth image of northern Egypt showing landscapes and water bodies. The black dashed thin line indicates the international border. The studied Wadi is shown by a red polygon.

This paper aims to (a) apply several quantitative, morpho-tectonic indices to examine quaternary tectonic evolution, (b) investigate tectonic anomalies due to tectonic changes and, (c) expand our knowledge about morphological changes and the effect of seismic hazards. While the relative tectonics of Wadi Al-Arish are not yet well recognized, studies on tectonic geomorphology aid in understanding recent tectonic signals and anomalies.

2. Study Area

The Wadi Al-Arish catchment is in northern Egypt and covers most of the Sinai Peninsula. It flows northward to the Mediterranean Sea (Figure 1). The mouth of Wadi Al-Arish is occupied by Al-Arish City. The Wadi Al-Arish catchment is located between 29°00' and 31°00' N and 33°05' and 34°45' E, covers ~23,300 km², and occupies ~36% of the total area of the Sinai Peninsula. Mostly, water tributaries come from Sinai (~91%) and a few drain from the neighboring El-Naqb Desert [15–17]. Wadi Al-Arish drains the central highlands of the Peninsula and its upstream courses come from El-Egma and El-Teeh plateaus [16].

The geology of the Sinai Peninsula has been investigated, defined, and mapped by many researchers [18–21]. The local lithology of Wadi Al-Arish has been remapped based on previous works and geological maps of Egypt prepared by Conoco and General Petroleum Corporation of Egypt [18] (Figure 2). The oldest exposed surface lithology in Wadi Al-Arish belongs to the Jurassic age, represented by Safa and Masajid Formations and made up of coal-bearing continental clastics with some marine carbonates with a few fossils, and marine shelf limestone with shale intercalations at the base. The Lower Cretaceous age is represented by the Risan' Aneiza Formation, which is composed of basal sandstone and conglomerate overlain by interbedded clastic and carbonate. The Upper Cretaceous is represented from the oldest to the youngest by undifferentiated deposits; the Raha Formation, Matulla Formation, and Suder Formation, respectively. The basal unit of the Upper Cretaceous is made up of clastic and biogenetic carbonate comprising Raha, Wata, Matulla, Qusier, and Duwi Formations. The Raha Formation consists of fossiliferous limestone with shale intercalations and oyster beds. The Matulla Formation consists of marine sandstone, marl, and shale. The Suder Formation was recognized as the youngest lithology of the Upper Cretaceous age, and consists of uniform marine chalk with thin shale intercalations. In Wadi Al-Arish, the Tertiary is represented by three units. They are arranged from base to top as the Esna Formation, which is composed of greenish-grey open marine shale, the Thebes Group (Egma Formation) that consists of bedded marine chalky limestone with a chert band, and the Plio-Pleistocene deposits comprising the Shagara and Marsa Alam Formations. The Quaternary deposits of the Wadi Al-Arish are represented by undifferentiated Quaternary deposits, stabilized dunes, wadi deposits, and sand dunes from the base to top, respectively. Figure 2 illustrates the geology of the entire study area.

Historical and instrumental seismicity of the Sinai Peninsula have been investigated by many researchers [22–27]. Twenty-five seismic events have been reported between 95 BC and 1910 AD at various localities with different intensities [28]. The reported intensities were based on recorded damage, which indicates heterogeneous behavior in space or time (Figure 3). Instrumentally, earthquakes have been reported in Egypt since 1903, and seismographs have been used since 1962 by the installing an observation station in the Helwan area, south of Cairo [24]. In the Sinai Peninsula, signals of earthquakes were recorded from 1900 to 1997 from a number of seismological stations. The main earthquakes of Sinai and surrounding areas are illustrated in Figure 3.

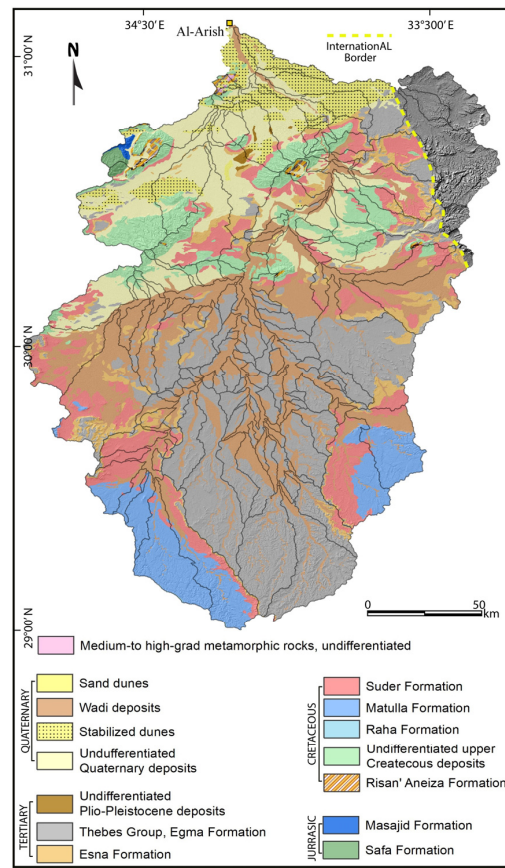


Figure 2. Detailed lithological map of the study area overlain by classified catchments/sub-catchments, modified after Reference in [18].

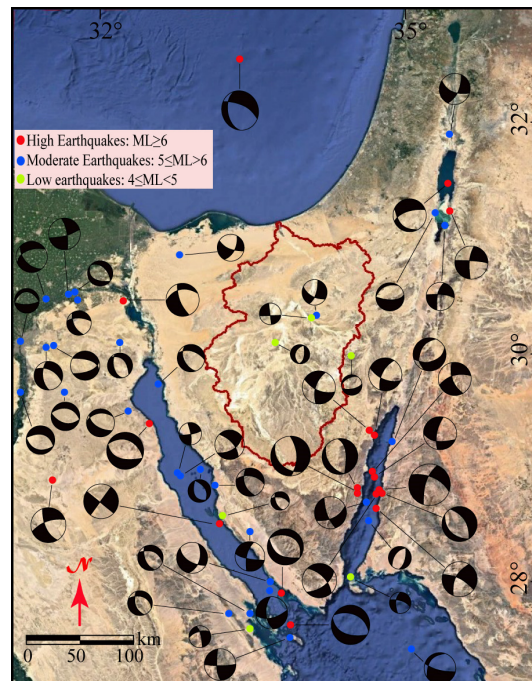


Figure 3. Distribution of historical and instrument-monitored earthquakes that have affected Sinai. The focal mechanisms are illustrated for each earthquake. The red polygon indicates Wadi Al-Arish area.

Tectonically, the Sinai sub-plate is a triangular continental block bounded between the African and Arabian plates and the Anatolian microplate [13,29–31]. The Sinai sub-plate is locked eastward by the sinistral transform Dead Sea fault and its extension in the Gulf of Aqaba. Recent remarks and evidence from marine geophysical studies identify the Gulf of Suez and its northward extension as the western boundary of the Sinai sub-plate [13,26,32]. The motion of this sub-plate is still under debate [13,14]. Regarding the motion of Sinai relative to the African plate, seismological and GPS studies indicate the dominance of slab-pull motion rather than ridge push forces [14]. Author of [14] indicates that the southern part of the Gulf of Suez is dominant by an extensional regime accompanied by sinistral motion, which is in agreement with the kinematic models of the authors [33–35]. The splitting of the Sinai sub-plate from the African plate in the Miocene within the Red Sea opening event frameworks, has continued to the present time [36–38]. The Suez rift was opened and linked to the Red Sea in the Miocene period [39,40]. Generally, the latest Miocene provides evidence of reducing tectonic activity along the Suez rift zone [13,37] concurrent with the Aqaba rift opening [13]. The movement of the Sinai sub-plate relative to the Dead Sea transform fault is estimated to be about 8–9 mm/year [41]. On the other hand, about 1 mm/year was recorded for the extensional motion along the Gulf of Suez rift [37,42]. The general tectonic styles and trends of faulting provide four main structural frameworks observed in the central and northern Sinai sub-plate, and the Suez and Aqaba gulfs [13]. The Wadi Al-Arish region has different morphological features according to its tectonic and topographic setting, in addition to lithological types [17]. The authors of [16] stated that morphological variations, including differences in elevation and position, are the main cause of variance in temperatures during a given season. Structurally, the Wadi Al-Arish region is highly affected by different structural elements (Figure 4). In the central part, two prominent structural features can be recognized. These are the Minsherah Abu kandu and the Ragabet El-Naam Shear zones cross Wadi Al-Arish providing NE-SW and E-W trends, respectively with a variable displacement up to 2.5 km [43,44] (Figure 4). This shear zone references the southernmost edge of the Early Mesozoic passive continental margin and the Syrian Arc tectonic front in the north [13,43]. Fractures/Faults over the study area indicate two main fractures systems with NW-WNW and NE-ESE trends. The authors of [17,45] state that these fractures and/or faults play an important role in the incision and trending of the majority of drainage systems. For example, over the southern part of Wadi Al-Arish there is compatibility between major trending of the faults/fractures and the main courses of the water systems. In the northern province that comprises Wadi Al-Arish, the deformation style has complex tectonics and large uplifting blocks of Mesozoic anticline folds oriented mostly N65°–85°E, as a result of the Syrian Arc System major tectonic [13] (Figure 4) [17]. Based on microtectonic analysis of the northern province by [46,47] the Cretaceous/Paleocene shortening structures were initiated from E-W to WNW-ESE by horizontal compression. The Gulf of Suez rift zone has NW-oriented normal faults of varying lengths in the Phanerozoic cover [13]. In addition, the basement rocks are fractured by strike-slip faults with subordinate normal and reverse offsets [13]. Based on a focal mechanism solution and shear analysis, the tectonic style in the Gulf of Aqaba was investigated and modeled, characterizing compressional strain accompanied by sinistral motion faults [34,48,49].

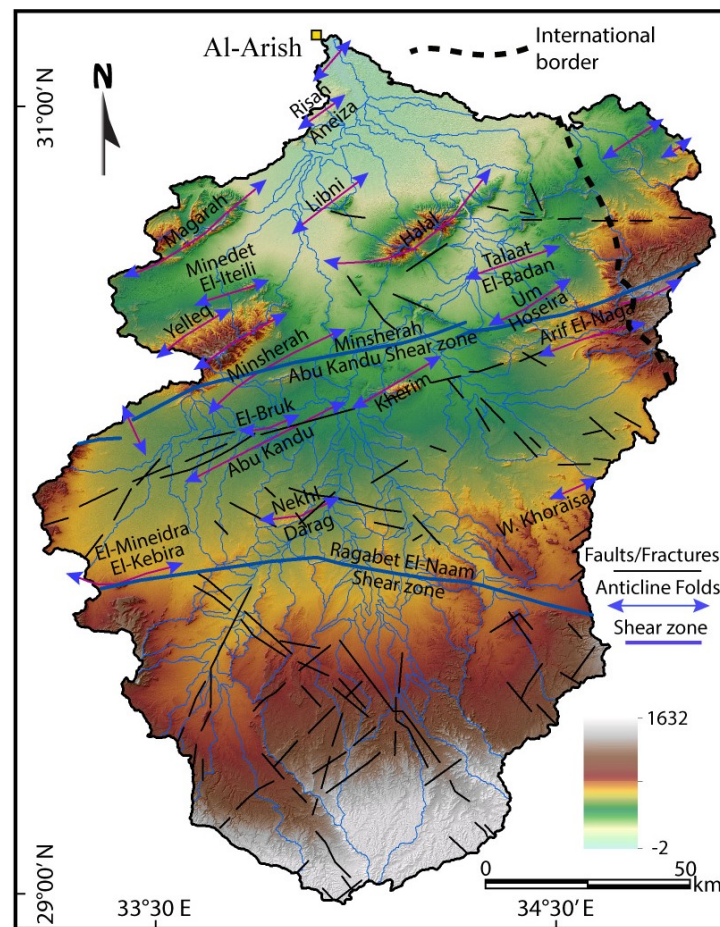


Figure 4. Shaded relief image (data from SRTM-30 resolution) of Wadi Al-Arish showing fractures, folds, and shear zones; modified after [18]. Blue hollow polygons indicate the classified catchments/sub-catchments of the study area.

3. Data and Methods

Raster and vector data (DEM and topographical maps) data were processed extract the different morpho-tectonic data. According to [50], catchments can be classified based on sizes into major catchments ($\geq 100 \text{ km}^2$) and sub-catchments ($< 100 \text{ km}^2$) (Figure 5). Basic geometric parameters including area, perimeter, and average elevation were extracted for the watersheds of the study area to provide preliminary dimensions of the different watersheds (Table S1, see Supplementary data). The watersheds were classified and recognized into 146 catchment/sub-catchment utilization greater than the fourth order.

Generally, geomorphic indices provide a quantitative method for deeper interaction between erosion and depositional processes, including river systems, valley morphology, and crossing profiles, as well as tectonically controlled features such as fault walls and extensions [6]. Active tectonic indices may result in anomalous signals along mountain scarps or in drainage systems [6,7,9,51]. These anomalies can be recorded by many local change signals from uplifting and subsidence movements [6]. This section is designed to calculate several geomorphic indices in catchments/sub-catchments of the Wadi Al-Arish major catchment (Figure 1) and classify them into different tectonic classes according to values of each index. Following the approach of [6,7], the resulting classes of each index are summed and divided into classes of relative seismic activity.

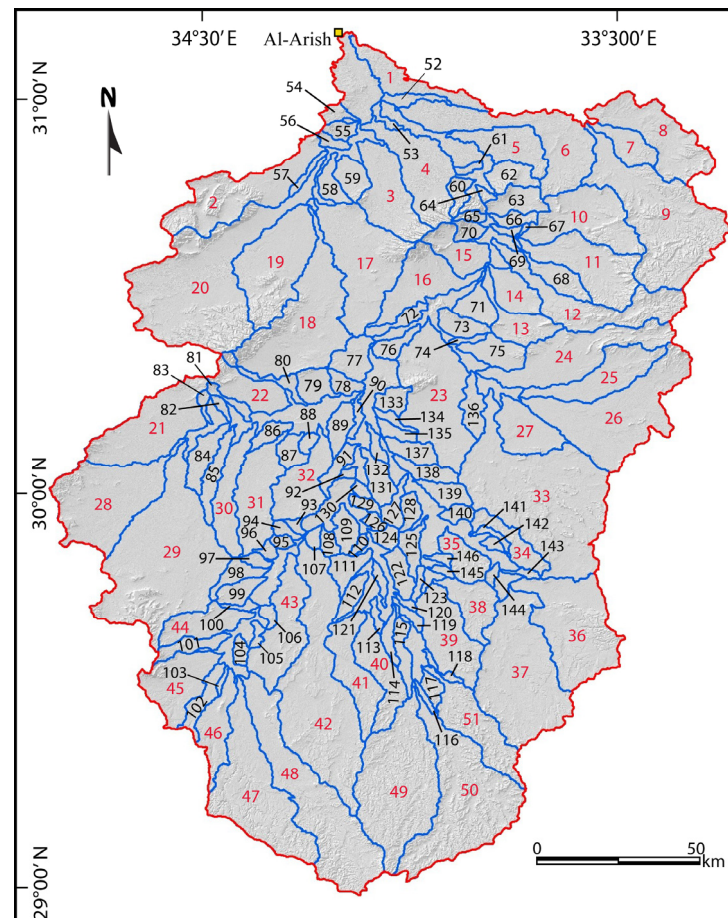


Figure 5. Shaded relief image (data from SRTM-30 resolution) of Wadi Al-Arish showing catchments/sub-catchments. Red numbers indicate catchments (1–51); black numbers indicate sub-catchments (52–146).

3.1. Stream Length-Gradient Index (SL)

Topography development results from an interaction between erosion processes such as rivers and streams over lithology with different rock strengths and soils [6,52]. The interaction eventually provides a dynamic equilibrium [6]. The stream length-gradient index (SL) was first recognized by [52] while studying the role of the strength of rocks and soils in rivers of the Appalachian Mountain zone in a region of the southeastern part of the United States [6]. This index is calculated as:

$$SL = (\Delta h / \Delta l)l$$

where $(\Delta h / \Delta l)$ describes the local slopes of the streams being studied and l is the stream length from the dividing point against midpoint center of the stream reach. The SL index is a very effective parameter to assess relative tectonic signals. Usually, this index gives values increasing along channels running over active spots and provides low values when these run parallel to structural elements initiated by major tectonics such as strike-slip faults [53].

3.2. Asymmetric Factor Index (Af)

The asymmetry factor (Af) is a parameter used to examine tectonic tilting along a water system. The index can be calculated over a large region [6,54]. Af is calculated from:

$$Af = 100(A_r / A_t)$$

where A_r indicates the area of the catchment to the right of the main trunk stream, and A_t represents values of the total area of the drainage catchment. If the A_f factor value is close to 50, the catchment has little or no tilting with stable conditions of development. The authors of [6,55,56] state that an A_f factor below or above 50 may result from catchment tilting, lithological structural control or active tectonics. In this paper, the values of A_f are calculated as $A_f - 50$, and provide the difference value between the observed value and the neutral value of 50.

3.3. Hypsometric Integral Index (H_i)

The hypsometric integral index reflects the distribution of different elevations in a landscape [57,58]. This index is calculated for a particular catchment area [7]. The H_i index is described as the area below the hypsometric curves, and thus defines the catchment volume that has no erosion evidence. The basic formula for calculating this index [54,55,59] is:

$$H_i = (\text{Elev}_{\text{Mean}} - \text{Elev}_{\text{Min}}) / (\text{Elev}_{\text{Max}} - \text{Elev}_{\text{Min}})$$

where mean, maximum, and minimum elevation points are extracted from a digital elevation model using geospatial analysis software. The hypsometric integral is not direct evidence for relative active signals. The hypsometric integral index provides convex curves in the lower part and concave to convex in addition to convex in the upper part.

3.4. Drainage Basin Shape Index (B_s)

The shape of basins is an indicator of tectonic activity. In active tectonic areas, relatively young basins have elongated shapes that are normal to topographic mountain slopes [6,60,61]. On the other hand, with less active tectonic signals, the basins have shapes that tend to be semi-circular to circular. The basin shape index may be expressed by the following equation:

$$B_s = B_l / B_w$$

where B_l indicates the basin length extended between its headwaters and mouth [9], while B_w describes the basin width at the basin widest strip. Regarding tectonic activity evaluation, high values of B_s index indicate elongation basins and indicate high tectonic activity. B_s lower values have a more circular-shaped basins with low levels of tectonic activity.

3.5. Valley Floor Width to Valley Height Ratio Index (V_f)

The V_f index is the ratio of the valley width to valley average height, [55]. This index is calculated from the following equation:

$$V_f = 2V_{fw} / [(E_{ld} - E_{cs}) + (E_{rd} - E_{cs})]$$

where V_{fw} describes the width of the valley floor, E_{ld} indicates the elevation of the left valley wall, E_{rd} indicates the elevation of the right valley wall, and E_{cs} is the average valley floor elevation. The V_f index discriminates between U-shaped valleys and V-shaped valleys. U-shaped valleys have high values of V_f , while V-shaped valleys have low V_f values. It is known that incision rate is associated with uplifting rate [7], and can be applied to describe active tectonics. Accordingly, low V_f values indicate a high rate of uplifting and incision, while high values of V_f indicate low uplifting and incision rates [62].

3.6. Mountain Front-Sinuosity Index (S_{mf})

The mountain front sinuosity index (S_{mf}) is used to clarify the interaction between erosion processes and tectonic actions. Erosive processes tend to produce more sinuous mountain fronts through rivers and streams, whereas active tectonics result in straight fronts, often associated with active geological structures [63,64]. This index is derived by:

$$S_{mf} = L_{mf} / L_s$$

where L_{mf} defines the total length of the mountain front along the mountain foot, while L_s measures the straight line of the mountain front. Values of Smf are calculated from aerial photography or topographic maps. However, the value extracted depends on the scale [63]. For more accuracy, large scale topographic maps are used to extract the Smf index values. The value of this index is used to differentiate between tectonically active fronts and fronts that are produced by erosional processes.

4. Results and Discussion

4.1. Morphotectonic Indices

4.1.1. Stream Length-Gradient Index (SL)

Values of the stream length-gradient index over the entire study area, extracted from a 30-m resolution digital elevation model and geospatial analysis are illustrated in Figure 6. SL values were computed every 100 m over the main rivers and streams. Generally, in order to define and classify different values of the index related to rock strength, various types of rock resistance were recognized, from low rock resistance (silt, marl, sand, alluvial deposits, and consolidated conglomerate), moderate rock resistance (schist and fillite, calcareous sandstone, and travertine), to high rock resistance which are low level metamorphisms (marble) [6,7].

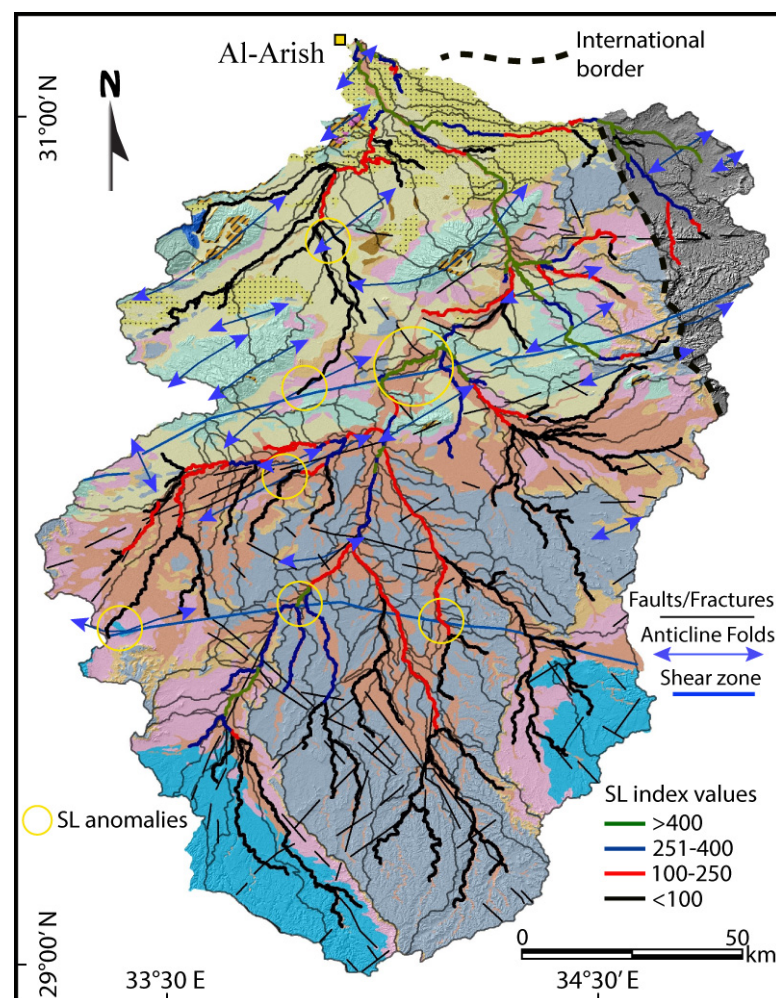


Figure 6. SL index along the drainage network of the study area. For lithological legend and catchments number, see Figures 3 and 5, respectively.

In this study, we observed that nearly all the lithology of the study area shows the same level of rock resistance [1,5,7]. Therefore, we assume that the role of rock strength is

negligible and that anomalies are related tectonic signatures. The SL index showed many tectonic anomalies, particularly along the channels running over shear zones in the middle part of the study area. Anomalies were observed due to high values over tectonic elements and low values over active spots (Figure 6). Values of the SL index had variable distribution over the whole study area. The highest and most anomalous values were observed along the Minsherah Abu Kandu shear zone in the middle zone of the proposed area. Various spots over the southern part of the study area had anomalously low SL index values over various trending fractures (Figure 6). In the northern part, the lowest values of the SL index, which were anomalously low for the area, occurred where the streams crossed the Libni anticline fold. Along the southern portion of the study area, the SL index tended to have relatively low values. An anomalous value of this index over a river parallel to Regabet El-Naam shear zone was recorded due high values over a stream running over a shear zone (Figure 6). Over the middle area, between the Minsherah Abu Kandu and Regabet El-Naam shear zones, the values of the SL index were mainly low. A few higher SL index values were related to tectonic signals. Along the Abu Kandu anticline fold, the SL index had anomalously low values crossing the fold.

4.1.2. Asymmetric Factor Index (Af)

The values of Af-50 varied from -0.7 in sub-catchment 88 to -28.3 in sub-catchment 125. Based on this index, the catchments/sub-catchments were defined into four classes: class 2 (nine catchments and 27 sub-catchments), class 3 (18 catchments and 29 sub-catchments), and finally class 4 (20 catchments and 36 sub-catchments). To evaluate relative active tectonics using this index, we calculated the absolute difference (values of Af-50) from 1 to 146 catchments/sub-catchments. Structurally controlled features, such as orientation of bedding, may provide an important impact of the asymmetry of the different catchments [7]. Accordingly, we observed Af anomalies in the Magarah fold in the northwestern part of the study area [9]. The results for this index are shown on Table S1 in the Supplementary data.

4.1.3. Hypsometric Integral Index (Hi)

We investigated Hi values and Hi curves. The Hi integral index values were between 0.30 in sub-catchment 57 and 0.51 in sub-catchments 56, 69, 94, 97. Our hypsometric analysis showed some concave curves associated with values of 0.48 and 0.49 (results of hypsometric curves are illustrated in Figure 7). Obtaining elevation values from digital elevation models are necessary for computation of this index. The hypsometric integral values do not relate directly to relative tectonic activity [6]. The value of this index is generally affected by rock strength as well as some other parameters. High values of the Hi index generally suggest a younger landscape that may developed by active tectonic events [7] (Figure 7). High Hi values may also result from very recent incisions into a young surface resulting from deposition processes. The authors of [6,7,9] assumed that convex lower part curves may indicate uplift signals along an active fault, or uplifting signals resulting from recent folding events. They also stated that Hi values greater than 0.5 result in convex curves. Values descending from 0.5 to 0.4 indicate convex-concave or semi straight curves, and values less than 0.4 are described by concave shapes (Figure 7). The hypsometric integral index values were analyzed based on the utilization of all catchments/sub-catchments of greater than the fourth drainage network order. Results for the hypsometric index are presented on Table S1 in the Supplementary data.



Figure 7. Hypsometric curves of the catchments. (A) Total surface of the catchment. (a) Surface area within the catchment above a given line of elevation (h). (H) Highest elevation of the catchment.

4.1.4. Drainage Basin Shape Index (Bs)

The drainage basin shape index was calculated for 146 catchment/sub-catchments. The lowest Bs index value was recorded for catchment 15 in the northern part of the study catchment, while the highest value was calculated for sub-catchment 115 in the southern part of the study catchment, as 0.6 and 6.5, respectively. Generally, relatively young

catchments of active regions tend to have elongated shapes normal to general topographic slopes. The shapes of elongation catchments that provide lower tectonic signatures tend to be circular [7,63]. High B_s values occur in elongation catchments, associated with relative higher tectonic signals. A high rate of uplifting along mountain fronts results in steep and elongated basins [65]. On the other hand, low B_s values are indicative of a more circular-shaped catchments associated with relative low tectonics and widening of the catchments produced from the mountain front [63,65]. Results of B_s index are listed on Table S3 in the Supplementary data.

4.1.5. Valley Floor Width to Valley Height Ratio Index (V_f)

Values of the V_f index vary with many factors, such as catchment size, rock type, and stream discharge [6]. Thus, V_f values should be estimated and calculated for similar geological conditions [7]. Values of this index were extracted along the main rivers of each catchment/sub-catchment over the entire study area, with a distance between ~0.1 and 1 km depending on the size of the catchments/sub-catchments examined. The lowest V_f value was recorded for sub-catchment 56 as 0.58 in the northern part, and the highest value was estimated for sub-catchment 86 as 20.33 in the middle part of the study area. Results for this index are shown in Table S4 in the Supplementary data. Both the lowest and highest values were incised in similar geological conditions. The authors of [66] calculated V_f index values in the SE Spain and suggested that valleys with V_f values >1 indicate tectonic quiescence and major lateral erosion, and values <1 indicate active tectonic uplifting. The work in [1] was carried out in central Anatolia in Turkey and stated that values >1.5 indicate high activity, values between 1.5 and 2.5 moderate activity, and values >2.5 low activity.

4.1.6. Mountain Front-Sinuosity Index (S_{mf})

Values of the mountain front sinuosity index relate to active tectonics along different fronts. In our work, 83 mountain segments were examined and evaluated (Figure 8). Values of the S_{mf} index were between 1.02 and 3.25. Results are shown in Table S5 in the Supplementary data. The lowest S_{mf} index value was observed along the middle-western part of the study area (front segment 46) coincidental with the southern segment of the Ragabat El-Naam shear zone and El-Mineidra El-Kebira anticline fold. However, all front segments had relatively low S_{mf} values along the Ragabat El-Naam shear zone. The highest value of the S_{mf} index was calculated for segment 15 in the western part of the study area. The examined fronts of the study area are illustrated in Figure 8 and may be classified into three main segment trends groups: front segments along the Minsherah Abu Kandu and Ragabat El-Naam shear zones trends (e.g., segments 8, 9, 19, 22, 23, 44, and 46) showing a nearly E-W trend; segments showing NW-SE trends (e.g., fronts 6, 21, 24, 25, 59, 77, and 80) and observed mainly in southern and eastern parts of the study area, and fronts showing NE-SW trends such as segments 14, 15, 48, 66, 69 and 71. In most active tectonic fronts, values are 1.0, and increase if uplift is ceased and erosional processes prevail. Lower S_{mf} values (1–1.5) indicate active tectonic fronts [1,9,67,68], while higher values of S_{mf} (>2.5) indicate active fronts [1,68]. The authors of Ref. [6] calculated this index in southern Spain using a digital elevation model, and acquired S_{mf} values between 1.04 and 1.61. Values below 1.1 indicated active tectonic signals, and values above 1.5 indicated inactive fronts. The relative tectonic activity of the eastern Betic Cordillera was evaluated by the authors of [66] by applying this index, and they recorded S_{mf} values from 1.17 to 3.51. Values lower than 1.4 indicated active tectonics signals, while values greater than 3 indicated low activity fronts.

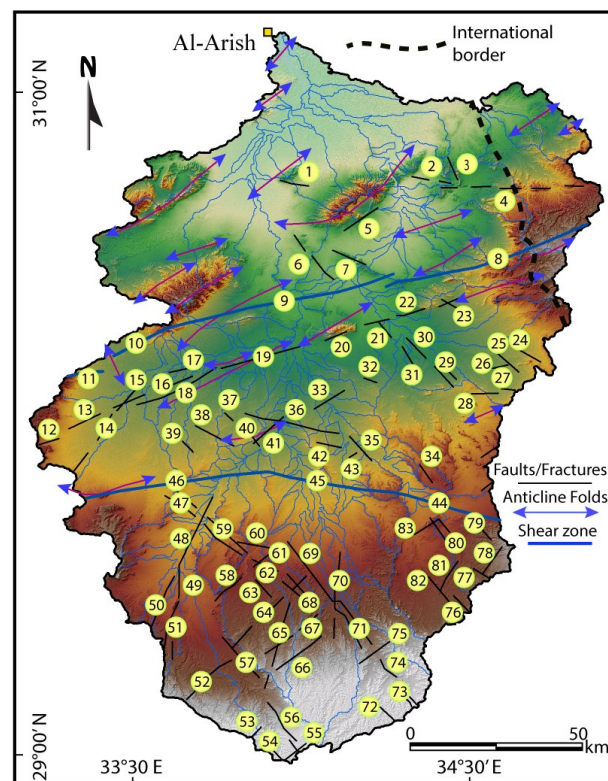


Figure 8. Map of mountain front sinuosity (Smf) locations and 83 mountain front segments for the Smf index.

4.2. Relative Tectonic Activity Levels Discussion

The application of morpho-tectonic indices along continental-scale features has been discussed in many studies [6,57,63,69,70]. Various analyses have been applied to the relationship between two morphometric indices (Smf and Vf) to present a primary quantitative model of the levels of tectonic activity of mountain fronts. Combining these two indices indicates tectonic activity classes [1,6,62,63,66]. Accordingly, some researchers have modeled a relationship between Smf and Vf values showing the distribution of these values along main rivers and streams, and along front segments [5,63,66]. In our research, we calculated morpho-tectonic indices for better landscape evaluations regarding tectonic activity levels. Generally, the indices have been classified by relative tectonic signals detected over the entire catchment [6,7,63,67,69]. In the present study, we applied the method of [6] that evaluates each index of a particular class of activity to model the relative tectonic activity classes of the Wadi Al-Arish catchment. To check the validity of our method, we probed many recent works. Relative tectonic classes were investigated along the southwest border of the Sierra Nevada in southern Spain by the authors of [6]. The boundaries of the studied levels changed with a single index; thus, for the purpose of this study, the boundaries selected were generally matched with changes in the various index value ranges. In this study, we focused only on areal features (catchments and sub/catchments) and averaged the results from the same bodies or features. In addition, many researchers (e.g., [9,70]) state that studying catchments may indicate uplift and subsidence signals and rates, and the origin of seismicity. The calculated indices were arbitrarily classified into three classes: high tectonic activity expressed (class 1), moderate tectonic activity named (class 2), and low tectonic activity (class 3). In this study, a new major average index (A/L) was defined as the relative tectonic activity level (RTAL) and estimated for all studied indices with four levels: level 1 defining very high tectonic activity signals (A/L between 1 and 1.5); level 2 with high tectonic activity signals ($2 \geq A/L > 1.5$); level 3 with moderately active tectonics signals ($2.5 \geq A/L > 2$), and level 4 with low tectonic activity signals ($A/L > 2.5$) (Table 1). The

average indices of A/L and values of RTAL are shown in Table 1 for 146 catchments/sub-catchments of Wadi Al-Arish (check Figure 4 for catchments/sub-catchments positions and locations).

Table 1. Classification of the RTAL (relative tectonic activity levels) in Wadi Al-Arish.

Catch.	A/L	RTAL	Catch.	A/L	RTAL	Sub-C.	A/L	RTAL
1	1.80	2	50	2.25	3	98	2.50	4
2	2.75	4	51	1.75	RTAL	99	3.00	4
3	2.50	4	Sub-C.	A/L	2	100	2.50	4
4	2.25	4	52	2.00	4	101	2.50	4
5	2.75	4	53	2.25	4	102	1.75	2
6	2.50	4	54	2.50	3	103	1.75	2
7	3.00	4	55	2.25	2	104	2.25	3
8	1.75	2	56	2.00	4	105	1.75	2
9	1.75	2	57	2.50	4	106	2.25	3
10	1.75	2	58	2.75	4	107	2.00	2
11	2.75	4	59	2.75	4	108	2.50	4
12	2.50	4	60	2.75	3	109	2.75	4
13	2.50	3	61	2.25	4	110	1.50	1
14	2.50	4	62	2.75	3	111	2.50	4
15	2.50	3	63	2.50	2	112	2.50	3
16	2.25	3	64	2.00	2	113	2.00	2
17	2.25	4	65	2.00	3	114	1.75	2
18	2.50	4	66	2.25	4	115	2.00	2
19	2.25	3	67	2.75	2	116	2.25	3
20	2.75	4	68	2.00	2	117	2.25	4
21	2.50	4	69	2.00	4	118	2.00	2
22	2.50	4	70	2.50	4	119	1.75	2
23	2.75	4	71	2.75	2	120	2.75	4
24	2.50	4	72	1.75	3	121	2.00	2
25	2.50	4	73	2.25	2	122	2.50	4
26	2.25	3	74	1.75	3	123	1.50	1
27	2.25	3	75	2.25	4	124	2.50	4
28	2.50	4	76	2.50	4	125	2.00	2
29	2.75	4	77	2.50	4	126	2.25	3
30	2.25	3	78	2.50	2	127	2.50	4
31	2.50	3	79	2.00	3	128	1.75	2
32	2.00	4	80	2.25	4	129	2.25	3
33	2.50	3	81	2.75	2	130	2.75	4
34	2.00	2	82	2.00	4	131	2.00	2
35	2.25	3	83	2.50	2	132	2.50	4
36	2.00	2	84	1.75	3	133	2.75	4
37	2.50	3	85	2.25	3	134	2.25	3
38	2.50	3	86	2.25	4	135	2.00	2
39	2.50	3	87	2.75	3	136	2.50	4
40	2.50	3	88	2.25	4	137	2.50	3
41	1.75	2	89	2.50	3	138	2.25	3
42	2.00	2	90	2.25	3	139	2.75	4
43	2.00	2	91	2.25	3	140	1.75	2
44	2.75	4	92	2.25	4	141	2.25	3
45	2.25	3	93	2.75	3	142	2.25	3
46	2.50	3	94	2.25	3	143	2.25	3
47	2.25	4	95	2.25	2	144	2.50	4
48	2.25	3	96	1.75	3	145	2.00	2
49	2.25	4	97	2.25	4	146	2.50	4

The Wadi Al-Arish catchment was investigated using morpho-tectonic indices for the first time, and low tectonic activity signals covered the largest parts of the study catchment. The tectonic analysis show that the high values (low tectonic signals) for the RTAL were

observed in the north to northwest parts of Wadi Al-Arish region. Additionally, some of these signals were recorded in the south and northeast parts as well. Moderate tectonic levels were found mainly in the northeast part of the study region with some signals in the south and middle parts. The RTAL index indicated high tectonic activity varying from large occurrences to small in the northeast, south, southeast, and north, respectively. High tectonic activity signals were recorded only in a very small part along the Ragabet El-Naam Shear zone. The distribution of the different tectonic activity levels is illustrated in Figure 6. Over the study region, level 4 (lowest tectonic activity level) covers 9701.79 Km² (47.52%) as estimated by RTAL; 31.91% (6515.26 km²) has moderate relative tectonic level as estimated by RTAL (class 3); high relative tectonic level (class 2) comprises (20.42 %) 4169.66 km²; while the smallest areas of the study region were recorded for class 1 (very high relative tectonic level), at 29.45 km² (0.14%). Therefore, half of the study area is covered by class 4 (low relative tectonic activity) and another half is divided mostly between class 3 and 2. Within different tectonic regions with greater active tectonic levels, the index values provided different estimations and classification ranges [6,7]. Accordingly, RTAL could also provide different values and boundaries between levels of relative tectonic activity. Our approach is based on regions that define different relative tectonic activity levels (Figure 9). The morpho-tectonic indices may reflect anomalies in the drainage systems or catchments/sub-catchments areal calculations [6,7,54]. These anomalies could be caused by the local tectonic signals resulted from uplifting or subsidence. Different anomalies were recorded in different regions. In [6,7] anomalies along mountain fronts and in drainage system in southern Spain and the Hindu Kush in northwestern Pakistan and NE Afghanistan, are discussed, respectively. The authors of [9] discuss anomalies along normal, active faults in the central eastern Desert of Egypt. In the present study, RTAL reflects a number of anomalies associated with structural control of folding and shear zones (Figure 9). Magarah, Libni, minsherah, Arif El-Naga, and El-Mineidra El-Kebira are folds associated with the lowest level of tectonic activity signals, and were recorded as RTAL anomalies.

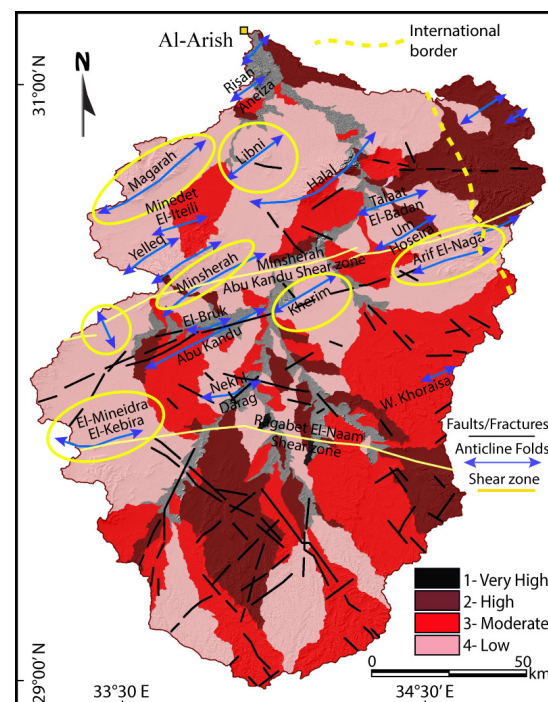


Figure 9. Distribution of the RTAL index of relative tectonics in the Wadi Al-Arish. Yellow polygons show the RTAL anomalies.

5. Conclusions

Studies on tectonic geomorphology, surface uplifting, and drainage catchments play a key role in present-day studies of active tectonic signals in intra-plates regions. Morpho-tectonic indices are very useful in evaluating the influence of active tectonics. These indices are advantageous, being computed from ArcGIS and remote sensing datasets over intra-plate regions to identify morpho-tectonic anomalies accompanied by active tectonics. This technique is valuable in the northern Sinai sub-plate where different tectonic types were observed, and no studies on active tectonics on absolute dates have been recorded. Based on values resulting from morpho-tectonic indices, including stream length-gradient (SL), the asymmetric factor (Af), the hypsometric integral (Hi), drainage basin shape (Bs), valley floor width to valley height ratio (Vf), and mountain front sinuosity (Smf) indices along Wadi Al-Arish in northern Sinai of Egypt, a combination overall index (RTAL) was developed and evaluated that was used to divide the studied landscape into four distinct levels of relative tectonic activity. Values of SL, Hi, and Bs indices were high along major tectonic elements in the study region. The values of Af ranged from -0.7 into -28.3 indicating a wide range of basin asymmetry due to tilt block tectonics. Low Vf values indicated that the various valleys are steep, deep, and narrow indicating a high rate of incision processes resulting from tectonic uplift. The Smf index had values between 1.02 and 3.25, indicating active tectonics for the majority of the mountain fronts. These indices are very effective for assessing seismic risk, and are estimated from ArcGIS software and remote sensing data as useful tools to recognize anomalies related to seismic activity. Analysis of relative tectonic activity based on the overall index (RTAL) was used to divide the Wadi al-Arish landscape into four levels of tectonic activity. The study area was mainly comprised of very low class 4 activity (47.52%), with tectonic activity ranging from large to small in the northeast, south, southeast, and north, respectively. Moreover, RTAL reflected many anomalies related to structural control of folding and shear zones, the lowest level of tectonic activity signals associated with the Magarah, Libni, minsherah, Arif El-Naga, and El-Mineidra El-Kebira folds. Finally, we applied a very effective method to test the hypothesis of relative tectonic activity assessment, but further, detailed evaluation is required for Quaternary geo-chronology and major tectonic element characteristics with significant major tectonic displacements.

Supplementary Materials: The following supporting information can be downloaded at: <https://www.mdpi.com/article/10.3390/app13042659/s1>.

Author Contributions: Conceptualization, M.E. and B.B.; methodology, A.A. and B.B.; software, M.E.; validation, M.E., H.B. and B.B.; formal analysis, M.E.; investigation, M.E. and A.A. resources, M.E. and B.B. data curation, M.E. and H.B. writing—original draft preparation, M.E. and B.B. writing—review and editing, A.A. and B.B. visualization, A.A.; supervision, B.B. project administration, B.B. funding acquisition, B.B. and A.A. All authors have read and agreed to the published version of the manuscript.

Funding: This research was supported by the Researchers Supporting Project number (RSP2023R296), King Saud University, Riyadh, Saudi Arabia.

Acknowledgments: This work was discussed, modified, and improved by the structural geology and tectonics lab in addition to the remote sensing lab of the Department of Geology, Faculty of Science, Al-Azhar University. The authors are grateful to Abdelrahman Khalifa, Al-Azhar University for his significant discussion and suggestion to improve this work.

Conflicts of Interest: The authors declare no conflict of interest.

References

1. Yildirim, C. Relative Tectonic Activity Assessment of the Tuz Gölü Fault Zone Central Anatolia, Turkey. *Tectonophysics* **2014**, *630*, 183–192. [[CrossRef](#)]
2. Takarada, S.; Bandibas, J.C. Volcanic Hazards Information and Assessment Systems. In *Forecasting and Planning for Volcanic Hazards, Risks, and Disasters*; Elsevier: Amsterdam, The Netherlands, 2021; Volume 2, pp. 565–584. [[CrossRef](#)]

3. Khalifa, A.; Bashir, B.; Alsalman, A.; Bachir, H. Morphometric-Hydro Characterization of the Coastal Line between El-Qussier and Marsa-Alam, Egypt: Preliminary Flood Risk Signatures. *Appl. Sci.* **2022**, *12*, 6264. [[CrossRef](#)]
4. Görüm, T. Tectonic, Topographic and Rock-Type Influences on Large Landslides at the Northern Margin of the Anatolian Plateau. *Landslides* **2019**, *16*, 333–346. [[CrossRef](#)]
5. Khalifa, A.; Çakir, Z.; Owen, L.A.; Kaya, Ş. Morphotectonic Analysis of the East Anatolian Fault, Turkey. *Turk. J. Earth Sci.* **2018**, *27*, 110–126. [[CrossRef](#)]
6. El Hamdouni, R.; Irigaray, C.; Fernández, T.; Chacón, J.; Keller, E.A. Assessment of Relative Active Tectonics, Southwest Border of the Sierra Nevada (Southern Spain). *Geomorphology* **2008**, *96*, 150–173. [[CrossRef](#)]
7. Mahmood, S.A.; Gloaguen, R. Appraisal of Active Tectonics in Hindu Kush: Insights from DEM Derived Geomorphic Indices and Drainage Analysis. *Geosci. Front.* **2012**, *3*, 407–428. [[CrossRef](#)]
8. Abdelazim, M.; Samir, A.; El-nader, I.A.; Badawy, A.; Hussein, H.; Castellort, S.; Whittaker, A.; Vergés, J.; Holbrook, J.; Schumm, S.A. Seismicity and Focal Mechanisms of Earthquakes in Egypt from 2004 to 2011. *NRIAG J. Astron. Geophys.* **1999**, *305*, 287–306. [[CrossRef](#)]
9. Khalifa, A.; Bashir, B.; Alsalman, A.; Ögretmen, N. Morpho-Tectonic Assessment of the Abu-Dabbab Area, Eastern Desert, Egypt: Insights from Remote Sensing and Geospatial Analysis. *ISPRS Int. J. Geo-Inf.* **2021**, *10*, 784. [[CrossRef](#)]
10. Sboras, S.; Lazos, I.; Mouzakiotis, E.; Karastathis, V.; Pavlides, S.; Chatzipetros, A. Fault Modelling, Seismic Sequence Evolution and Stress Transfer Scenarios for the July 20, 2017 (M W 6.6) Kos–Gökova Gulf Earthquake, SE Aegean. *Acta Geophys.* **2020**, *68*, 1245–1261. [[CrossRef](#)]
11. Roselli, P.; Marzocchi, W.; Mariucci, M.T.; Montone, P. Earthquake Focal Mechanism Forecasting in Italy for PSHA Purposes. *Geophys. J. Int.* **2018**, *212*, 491–508. [[CrossRef](#)]
12. Yang, J.; Xu, C.; Wen, Y.; Xu, G. Complex Coseismic and Postseismic Faulting During the 2021 Northern Thessaly (Greece) Earthquake Sequence Illuminated by InSAR Observations. *Geophys. Res. Lett.* **2022**, *49*, e2022GL098545. [[CrossRef](#)]
13. Masoud, A.A.; Koike, K. Morphotectonics Inferred from the Analysis of Topographic Lineaments Auto-Detected from DEMs: Application and Validation for the Sinai Peninsula, Egypt. *Tectonophysics* **2011**, *510*, 291–308. [[CrossRef](#)]
14. Badawy, A.; Mohamed, A.M.S.; Abu-Ali, N. Seismological and GPS constraints on Sinai sub-plate motion along the Suez rift. *Stud. Geophys. Geod.* **2008**, *52*, 397–412. [[CrossRef](#)]
15. Moawad, M.B. Analysis of the Flash Flood Occurred on 18 January 2010 in Wadi El Arish, Egypt (a Case Study). *Geomat. Nat. Hazards Risk* **2013**, *4*, 254–274. [[CrossRef](#)]
16. Kader, H.A. GIS Based Morphometric Analysis of Wadi El-Arish Watershed Sinai, Egypt-Using ASTER (DEM) Data. *Int. J. Sci. Eng. Res.* **2020**, *11*, 682–694.
17. Elbarbary, S.; Araffa, S.A.S.; El-Shahat, A.; Abdel Zaher, M.; Khedher, K.M. Delineation of Water Potentiality Areas at Wadi El-Arish, Sinai, Egypt, Using Hydrological and Geophysical Techniques. *J. Afr. Earth Sci.* **2021**, *174*, 104056. [[CrossRef](#)]
18. Corporation, C.; Conoco, G.P. *General Petroleum Corporation. Geological Map of Egypt, Scale 1:500,000*; Gebel Hamata: Cairo, Egypt, 1987.
19. Abdelsalam, M.G.; Stern, R.J. Sutures and Shear Zones in the Arabian-Nubian Shield. *J. Afr. Earth Sci.* **1996**, *23*, 289–310. [[CrossRef](#)]
20. Moustafa, A.R. Structural Setting and Tectonic Evolution of North Sinai Folds, Egypt. *Geol. Soc. Spec. Publ.* **2010**, *341*, 37–63. [[CrossRef](#)]
21. Abdelfadil, K.M.; Obeid, M.A.; Azer, M.K.; Asimow, P.D. Late Neoproterozoic Adakitic Lavas in the Arabian-Nubian Shield, Sinai Peninsula, Egypt. *J. Asian Earth Sci.* **2018**, *158*, 301–323. [[CrossRef](#)]
22. Ben-Menahem, A. Earthquake Catalogue for the Middle East (92 B.C.-1980 A.D.). *Boll. Geofis. Orca Ed. Appl.* **1979**, *21*, 245–310.
23. Poirier, J.P.; Taher, M.A. Historical Seismicity in the near and Middle East, North Africa, and Spain from Arabic Documents (VIIth-XVIIIth Century). *Bull. Seismol. Soc. Am.* **1980**, *70*, 2185–2201. [[CrossRef](#)]
24. Maamoun, M.; Megahed, A.; Allam, A. Seismicity of Egypt. *Bull. Helwan Inst. Astron. Geophys.* **1984**, *4*, 109–160.
25. Ambraseys, N.; Melville, C.R.A. *The Seismicity of Egypt, Arabia and the Red Sea: A Historical Review*; Cambridge University Press: Cambridge, UK, 1994.
26. Kebeasy, R.M. Seismicity. In *The Geology of Egypt*; Routledge: Abingdon, UK, 1990; pp. 51–59. [[CrossRef](#)]
27. Abu El Enean, K. A Study on the Seismotectonics of Egypt in Relation to the Mediterranean and Red Sea Tectonics. Ph.D. Thesis, Ain Shams University, Cairo, Egypt, 1997.
28. Abdel-Rahman, K.; Al-Amri, A.M.; Abdel-Moneim, E. Seismicity of Sinai Peninsula, Egypt Kamal Abdel-Rahman. *Arab. J. Geosci.* **2015**, *2*, 103–118. [[CrossRef](#)]
29. Joffe, S.; Garfunkel, Z. Plate Kinematics of the Circum Red Sea—a Re-Evaluation. *Tectonophysics* **1987**, *141*, 5–22. [[CrossRef](#)]
30. Le Pichon, X.; Francheteau, J. A Plate-Tectonic Analysis of the Red Sea-Gulf of Aden Area. *Tectonophysics* **1978**, *46*, 369–388. [[CrossRef](#)]
31. McKenzie, D.P. Plate Tectonics of the Mediterranean Region. *Nature* **1970**, *226*, 239–243. [[CrossRef](#)]
32. McKenzie, D. Active Tectonics of the Mediterranean Region. *Geophys. J. R. Astron. Soc.* **1972**, *30*, 109–185. [[CrossRef](#)]
33. Badawy, A. Present-Day Seismicity, Stress Field and Crustal Deformation of Egypt. *J. Seismol.* **2005**, *9*, 267–276. [[CrossRef](#)]
34. Badawy, A.; Horváth, F. Seismicity of the Sinai Subplate Region: Kinematic Implications. *J. Geodyn.* **1999**, *27*, 451–468. [[CrossRef](#)]
35. Mahmoud, S.; Reilinger, R.; McClusky, S.; Vernant, P.; Tealeb, A. GPS Evidence for Northward Motion of the Sinai Block: Implications for E. Mediterranean Tectonics. *Earth Planet. Sci. Lett.* **2005**, *238*, 217–224. [[CrossRef](#)]

36. Cochran, J.R. Northern Red Sea: Nucleation of an Oceanic Spreading Center within a Continental Rift. *Geochem. Geophys. Geosystems* **2005**, *6*, 3. [\[CrossRef\]](#)
37. Steckler, M.S.; Berthelot, F.; Lyberis, N.; Le Pichon, X. Subsidence in the Gulf of Suez: Implications for Rifting and Plate Kinematics. *Tectonophysics* **1988**, *153*, 249–270. [\[CrossRef\]](#)
38. McClay, K.; Khalil, S. Extensional Hard Linkages, Eastern Gulf of Suez, Egypt. *Geology* **1998**, *26*, 563. [\[CrossRef\]](#)
39. Bartov, Y.; Steinitz, G.; Eyal, M.; Eyal, Y. Sinistral Movement along the Gulf of Aqaba—Its Age and Relation to the Opening of the Red Sea. *Nature* **1980**, *285*, 220–222. [\[CrossRef\]](#)
40. Patton, T.L.; Moustafa, A.R.; Nelson, R.A.; Abdine, S.A. Tectonic Evolution and Structural Setting of the Suez Rift. In *Interior Rift Basins*; American Association of Petroleum Geologists: Tulsa, OK, USA, 1994. [\[CrossRef\]](#)
41. Garfunkel, Z.; Zak, I.; Freund, R. Active Faulting in the Dead Sea Rift. *Tectonophysics* **1981**, *80*, 1–26. [\[CrossRef\]](#)
42. Bosworth, W.; Taviani, M. Late Quaternary Reorientation of Stress Field and Extension Direction in the Southern Gulf of Suez, Egypt: Evidence from Uplifted Coral Terraces, Mesoscopic Fault Arrays, and Borehole Breakouts. *Tectonics* **1996**, *15*, 791–802. [\[CrossRef\]](#)
43. Abd El Samie, S.G.; Sadek, M.A. Groundwater Recharge and Flow in the Lower Cretaceous Nubian Sandstone Aquifer in the Sinai Peninsula, Using Isotopic Techniques and Hydrochemistry. *Hydrogeol. J.* **2001**, *9*, 378–389. [\[CrossRef\]](#)
44. Corchete, V.; Chourak, M.; Hussein, H.M. Shear Wave Velocity Structure of the Sinai Peninsula from Rayleigh Wave Analysis. *Surv. Geophys.* **2007**, *28*, 299–324. [\[CrossRef\]](#)
45. El-Ghazawi, M.M. Hydrogeological Studies in Northeast Sinai, Egypt. Ph.D. Thesis, Mansoura University, Mansoura, Egypt, 1989.
46. Letouzey, J.; Tremolieres, P. Paleo-stress Field around the Mediterranean since the Mesozoic from microtectonics. Comparison with plate tectonic data. In *Rock Mechanics*; Springer: Vienna, Austria, 1980; pp. 173–192. [\[CrossRef\]](#)
47. Eyal, Y.; Reches, Z. Tectonic Analysis of the Dead Sea Rift Region since the Late-Cretaceous Based on Mesostructures. *Tectonics* **1983**, *2*, 167–185. [\[CrossRef\]](#)
48. Mahmoud, S.M. Seismicity and GPS-Derived Crustal Deformation in Egypt. *J. Geodyn.* **2003**, *35*, 333–352. [\[CrossRef\]](#)
49. El-Fiky, G.S. GPS-Derived Velocity and Crustal Strain Field in The. *Bull. Earthq. Res. Inst. Univ. Tokyo* **2005**, *80*, 73–86.
50. Horton, R.E. Erosional Development of Streams and Their Drainage Basins: Hydrophysical Approach to Quantitative Morphology. *Bull. Geol. Soc. Am.* **1945**, *56*, 275–370. [\[CrossRef\]](#)
51. Bhattarai, I.; Gani, N.D.; Xue, L. Geomorphological Responses of Rivers to Active Tectonics along the Siwalik Hills, Midwestern Nepalese Himalaya. *J. Mt. Sci.* **2021**, *18*, 1268–1294. [\[CrossRef\]](#)
52. Hack, J.T. Stream-Profile Analysis and Stream-Gradient Index. *J. Res. Us Geol. Surv.* **1973**, *1*, 421–429.
53. Keller, E.A.; Pinter, N. *Active Tectonics: Earthquakes, Uplift and Landscape*, 2nd ed.; Prentice Hall: Upper Saddle River, NJ, USA, 2002.
54. Bhat, M.A.; Dar, T.; Bali, B.S. Morphotectonic Analysis of Aripal Basin in the North-Western Himalayas (India): An Evaluation of Tectonics Derived from Geomorphic Indices. *Quat. Int.* **2020**, *568*, 103–115. [\[CrossRef\]](#)
55. Ezati, M.; Gholami, E. Neotectonics of the Central Kopeh Dagh Drainage Basins, NE Iran. *Arab. J. Geosci.* **2022**, *15*, 992. [\[CrossRef\]](#)
56. Baruah, M.P.; Bezbaruah, D.; Goswami, T.K. Active Tectonics Deduced from Geomorphic Indices and Its Implication on Economic Development of Water Resources in South-Eastern Part of Mikir Massif, Assam, India. *Geol. Ecol. Landsc.* **2020**, *6*, 99–112. [\[CrossRef\]](#)
57. Cardoso, M.; da Silveira, A.S.; de Vargas, M.R.; de Oliveira, J.M.M.T.; Barbosa, D.V.E.; de Oliveira, L.F.B.; Fredere, A.C.; Lõndero, V. Geomorphic Expression of Shear Zones in Southern Brazilian and Uruguayan Shields. *Geomorphology* **2021**, *382*, 107678. [\[CrossRef\]](#)
58. Strahler, A. Dynamic Basis of Geomorphology. *Geol. Soc. Am. Bull.* **1952**, *63*, 923–938. [\[CrossRef\]](#)
59. Owen, L.A. 5.2 Tectonic Geomorphology: A Perspective. In *Treatise on Geomorphology*; Elsevier: Amsterdam, The Netherlands, 2013; Volume 148, pp. 3–12. [\[CrossRef\]](#)
60. Partabian, A.; Nourbakhsh, A.; Ameri, S. GIS-Based Evaluation of Geomorphic Response to Tectonic Activity in Makran Mountain Range, SE of Iran. *Geosci. J.* **2016**, *20*, 921–934. [\[CrossRef\]](#)
61. Faghih, A.; Samani, B.; Kusky, T.; Khabazi, S.; Roshanak, R. Geomorphologic Assessment of Relative Tectonic Activity in the Maharlou Lake Basin, Zagros Mountains of Iran. *Geol. J.* **2012**, *47*, 30–40. [\[CrossRef\]](#)
62. Khalifa, A.; Çakir, Z.; Owen, L.A.; Kaya. Evaluation of the Relative Tectonic Activity of the Adıyaman Fault within the Arabian-Anatolian Plate Boundary (Eastern Turkey). *Geol. Acta* **2019**, *17*, 1–17. [\[CrossRef\]](#)
63. Bull, W.B.; McFadden, L.D. Tectonic Geomorphology North and South of the Garlock Fault, California. In *Geomorphology in Arid Regions: A Proceedings Volume of the 8th Annual Geomorphology Symposium*; Doehring, D.O., Ed.; State University of New York: Binghamton, NY, USA, 1977; pp. 559–589.
64. Keller, E.A.; Pinter, N. *Active Tectonics: Earthquakes, Uplift, and Landscape*; Prentice Hall: Upper Saddle River, NJ, USA, 2002.
65. Ramirez-Herrera, M. Geomorphic Assessment of Active Tectonics in the Acambay Graben, Mexican Volcanic Belt. *Earth Surf. Process. Landf.* **1998**, *23*, 317–332. [\[CrossRef\]](#)
66. Silva, P.G.; Goy, J.L.; Zazo, C.; Bardaji, T. Fault-Generated Mountain Fronts in Southeast Spain: Geomorphologic Assessment of Tectonic and Seismic Activity. *Geomorphology* **2003**, *50*, 203–225. [\[CrossRef\]](#)
67. Rockwell, T.K.; Keller, E.A.; Johnson Donald, L. Tectonic Geomorphology of Alluvial Fans and Mountain Fronts near Ventura, California. In *Tectonic Geomorphology*; Morisawa, M., Hack, J.T., Eds.; Allen and Unwin Publishers: Boston, MA, USA, 1985; pp. 183–207.

68. Elnobi, M.; Bashir, B.; Alsalman, A.; Bachir, H. Geospatial Analytics for Preliminary Landscape Active Tectonic Assessment of the Wadi Araba Basin, Western Gulf of Suez, Egypt. *Appl. Sci.* **2022**, *12*, 12152. [[CrossRef](#)]
69. Azor, A.; Keller, E.A.; Yeats, R.S. Geomorphic Indicators of Active Fold Growth: South Mountain-Oak Ridge Anticline, Ventura Basin, Southern California. *Bull. Geol. Soc. Am.* **2002**, *114*, 745–753. [[CrossRef](#)]
70. Xue, L.; Gani, N.D.; Abdelsalam, M.G. Drainage Incision, Tectonic Uplift, Magmatic Activity, and Paleo-Environmental Changes in the Kenya Rift, East African Rift System: A Morpho-Tectonic Analysis. *Geomorphology* **2019**, *345*, 106839. [[CrossRef](#)]

Disclaimer/Publisher’s Note: The statements, opinions and data contained in all publications are solely those of the individual author(s) and contributor(s) and not of MDPI and/or the editor(s). MDPI and/or the editor(s) disclaim responsibility for any injury to people or property resulting from any ideas, methods, instructions or products referred to in the content.